CMS Physics Analysis Summary

Contact: cms-pag-conveners-exotica@cern.ch 2015/12/15

Search for new physics in high mass diphoton events in proton-proton collisions at 13 TeV

The CMS Collaboration

Abstract

We report on a search for new physics using high mass diphoton events. The search employs 2.6 fb^{-1} of pp collision data collected by the CMS experiment in 2015 at $\sqrt{s} = 13$ TeV and it is aimed at extradimensional models leading to resonant production of two photons. Limits on the production cross section of Randall-Sundrum gravitons decaying to two photons are obtained in the range 500-4500 GeV.

1 Introduction

The recent discovery of a Higgs boson [1, 2] with a mass of about 125 GeV by the CMS and ATLAS experiments poses the problem of the naturalness of the standard model (SM) of particle physics. The large difference between the scales of electroweak and gravitational interactions makes an unified theory unnatural, requiring large cancellation between quantum corrections to the Higgs boson mass and its bare value. This difficulty is known as the hierarchy problem. One approach to the problem is the introduction of additional space-like dimensions. This ansatz allows the solution of the hierarchy problem, lowering the effective Planck scale by "diluting" gravity in the additional dimensions.

Two families of models, introduced by Arkani-Hamed, Dimopoulos and Dvali (ADD) [3], and by Randall and Sundrum (RS) [4], have been developed in the past years. In the first, additional dimensions are assumed to be flat and compact. By allowing the gravitation field to propagate in the extra dimensions, the large difference between the Planck and electroweak scales can be explained. In the RS model, the presence of two brane-worlds is postulated and the SM fields are allowed to propagate in only one of the two. The further assumption of a warped space-time metric allows the difference between the electroweak and Planck scales to be accounted for. From the phenomenological point of view, both families predict that the excitation of the gravitational field leads to "towers" of spin-2 resonances, commonly denoted as gravitons, separated by a characteristic mass scale [5–9].

In this analysis, we search for the effect of extradimensional models in diphoton final states. In the case of the ADD model, the mass separation is so small that individual resonances cannot be resolved from each other. In the diphoton final state this leads to the observation of a broad excess in the invariant mass spectrum over the SM continuum. In the case of the RS model, the mass separation is large enough to allow the independent observation of each resonance. The search reported here is for the resonant production of two photons, thus focusing on RS models. ADD models will be investigated in a forthcoming analysis.

The phenomenology of the RS model is typically parametrised in terms of an effective coupling constant $\tilde{\kappa}$ expressed as $\tilde{\kappa} = \sqrt{8\pi}\kappa/m_{Pl}$, where κ is the curvature scale of the extra dimensions and $m_{Pl} \sim 10^{19}$ GeV is the Planck mass [9]. The relative width of the lowest graviton resonance is approximately $1.4\tilde{\kappa}^2$ and the total production cross section grows roughly as $\tilde{\kappa}^2$. In this search, the range $0.01 < \tilde{\kappa} < 0.2$ and resonance masses (m_{G}) between 500 GeV and 4.5 TeV are considered.

Similar searches were performed at lower centre of mass energies by the CMS and ATLAS collaborations in proton-proton collisions and by the CDF and D0 collaborations in proton-antiproton collisions, using final states containing pairs of photons, leptons, jets or vector bosons [10–19]. Here we extend the reach of the search for RS graviton signals exploiting the higher collision energy delivered by the LHC, employing 2.6 fb^{-1} of pp collision data collected by the CMS experiment at the CERN LHC in 2015 at $\sqrt{s} = 13$ TeV.

2 The CMS detector

The central feature of the CMS apparatus is a superconducting solenoid of 6 m internal diameter, providing a magnetic field of 3.8 T. Within the superconducting solenoid volume are a silicon pixel and strip tracker, a lead tungstate crystal electromagnetic calorimeter (ECAL), and a brass and scintillator hadron calorimeter (HCAL), each composed of a barrel and two endcap sections. Forward calorimeters (HF) extend the pseudorapidity [20] coverage provided by the

barrel and endcap detectors. Muons are measured in gas-ionization detectors embedded in the steel flux-return yoke outside the solenoid.

In the barrel section of the ECAL, an energy resolution of about 1% is achieved for unconverted or late-converting photons in the tens of GeV energy range. The remaining barrel photons have a resolution of about 1.3% up to a pseudorapidity of $|\eta| = 1$, rising to about 2.5% at $|\eta| = 1.4$. In the endcaps, the resolution of unconverted or late-converting photons is about 2.5%, while the remaining endcap photons have a resolution between 3 and 4% [21]. The dynamic range of the ECAL readout electronics allows to measure the energy deposited in single crystals in the barrel (endcaps) region between a few tens of MeV and roughly 2(3) TeV.

The particle-flow event algorithm [22, 23] reconstructs and identifies each individual particle with an optimised combination of information from the various elements of the CMS detector. The energy of photons is directly obtained from the ECAL measurement, correcting for radiative losses and containment effects. The energy of electrons is determined from a combination of the electron momentum at the primary interaction vertex as determined by the tracker, the energy of the corresponding ECAL cluster, and the energy sum of all bremsstrahlung photons spatially compatible with originating from the electron track. The energy of muons is obtained from the curvature of the corresponding track. The energy of charged hadrons is determined from a combination of their momentum measured in the tracker and the matching ECAL and HCAL energy deposits, corrected for zero-suppression effects and for the response function of the calorimeters to hadronic showers. Finally, the energy of neutral hadrons is obtained from the corresponding corrected ECAL and HCAL energy.

The first level (L1) of the CMS trigger system, composed of custom hardware processors, uses information from the calorimeters and muon detectors to select the most interesting events in a fixed time interval of less than 4 μs. The high level trigger (HLT) processor farm further decreases the event rate from around 100 kHz to around 300 Hz, before data storage.

A more detailed description of the CMS detector, together with a definition of the coordinate system used and the relevant kinematic variables, can be found in Ref. [20].

3 Data and simulated samples

The data considered in this analysis correspond to an integrated luminosity of 2.6 fb^{-1} collected by the CMS experiment in 2015. The dataset analysed fulfils standard quality criteria for all components of the CMS detector, except in a fraction of the dataset for the HF calorimeter.

Randall-Sundrum graviton resonances decaying to two photons were generated with PYTHIA, 8.2 [24] using the NNPDF2.3 [25] parton distribution functions (PDFs). Several samples were generated, spanning signal hypotheses in the range where 500 GeV $< m_{\mathrm{G}} <$ 4.5 TeV and $0.01 < \tilde{\kappa} < 0.2$.

The processes giving raise to background in the search for the diphoton decay of the RS graviton are the irreducible background from the direct production of two photons as well as the reducible components due to $\gamma +$ jets and multi-jet final states, where the jet fragments are misidentified as photons. Simulated background samples were used for optimisation of the analysis and to study the systematic uncertainties related to the background estimation. The background from prompt diphoton processes was generated using SHERPA 2.1 [26].
The MADGRAPH5, 2.2 [27] generator, interfaced with PYTHIA, was used to model the production of $\gamma +$ jets. In both cases additional hard emissions, up to three additional partons in the final state, were generated at leading order (LO) in perturbative QCD and the NNPDF3.0 [28]

PDFs were used. Multi-jet final states were modelled using PYTHIA with NNPDF2.3 PDFs. The PYTHIA tune CUETP8M1 [29] was used.

A detailed simulation of the CMS detector response to the events in the signal and background samples was performed using the GEANT4 package [30]. For the analysed data, the average number of interaction per bunch crossing is 11.4, with an RMS of 2.1. Simulated events include the effect of multiple proton-proton interactions (pileup) taking place each bunch crossing and were weighted to reproduce the distribution of the number of interactions per bunch crossing in data.

4 Event selection and reconstruction

Events with at least two reconstructed photon candidates are selected and a search is made for a localised excess of events in the diphoton mass spectrum consistent with the production of a graviton resonance.

The trigger selection requires at least two photon candidates of transverse momentum above 60 GeV. For these events, the ratio between the energy deposited in the hadron calorimeter towers behind each the photon candidate and the photon energy ("H/E ratio") is required to be lower than 0.15. The trigger selection is fully efficient for graviton resonances of mass above 500 GeV.

Photon candidates are reconstructed from energy deposits in the ECAL. Energy deposits compatible with the expected shower shape of electrons and photons are clustered together. The clustering algorithm does not make any hypothesis as to whether the particle originating from the interaction point is a photon or an electron. Thus the same algorithm used for photon reconstruction can be applied to $Z \to e^+e^-$ events and these events can be used to measure the efficiency of the photon selection criteria and of the photon energy scale and resolution.

In order to obtain the best energy resolution, the ECAL signals are calibrated and corrected for several detector effects. The variation of the crystal transparency during the run is corrected with a dedicated monitoring system and the single-channel response equalised using collision events [21]. For the dataset considered by this analysis, the single-channel response calibration coefficients derived during the 8 TeV LHC run, corrected for the response variation measured by the monitoring system, are used. Due to the uncertainty of such extrapolation, the resulting photon energy resolution is worse than that achieved for the 8 TeV run.

The containment of the shower in the clustered crystals, the shower losses for photons that convert in the material upstream of the calorimeter, and the effects of pileup, are corrected for using a multivariate regression technique [21]. Photons of very high energy can deposit in a single crystals higher energy than can be measured by the ECAL electronics. In this case, the estimated photon energy can be significantly lower than the true one and its variance very large. A dedicated multivariate regression was developed to correct for the effect. Using simulated events it is found that after the application of the corrections, the energy scale of photons where saturation of the ECAL electronics has occurred deviates from unity by less than 2% and the energy resolution is better than 3%. However, saturation occurred for none of the photon candidates selected in this analysis.

Photon candidates are organised in pairs, which are required to satisfy the following kinematic criteria:

- The p_T of both candidates is required to be above 75 GeV.

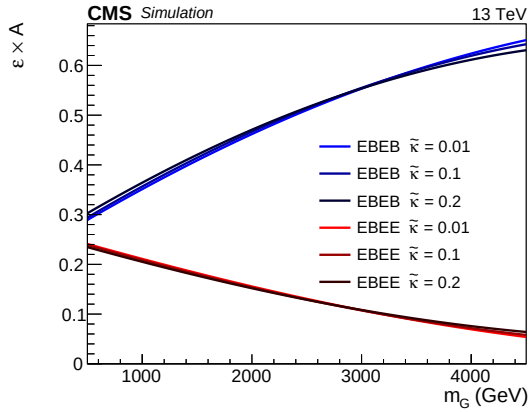

Figure 1: Fraction of RS graviton events selected by the two analysis categories for 500 GeV $<$ m_G $<$ 4500 GeV and $\tilde{\kappa} = 0.01, 0.1, 0.2$.

- The absolute value of the pseudorapidity of both candidates, computed with respect to centre of the CMS detector and denoted $|\eta_{SC}|$ in the following, is required to be below 2.5 and not between 1.44 and 1.57.
- At least one of the photon candidates is required to have $|\eta_{SC}|$ below 1.44 (i.e. events with both photon candidates in the ECAL endcaps regions are rejected).
- The invariant mass of the pair, $m_{\gamma\gamma}$, is required to be above 230 GeV. For events where one of the photon candidates is in the endcap region, $m_{\gamma\gamma} > 320$ GeV is required.

Photon candidates are further required to satisfy a set of identification criteria:

- The transverse size of the electromagnetic cluster is required to be compatible with that expected from prompt photons.
- The H/E ratio is required to be lower than 0.05.
- The sum of the transverse momenta (I_{Ch}) of particle-flow charged hadron candidates contained in a cone of radius 0.3 in η, ϕ space centred on the photon candidates is required to be below 5 GeV. Charged particle-flow candidates compatible with conversion tracks associated with the photon candidates are excluded from the sum.
- The sum of the transverse energy the additional photon candidates contained in the same geometric cones, corrected for pileup effects, is required to be below 2.5 GeV.
- Photon candidates associated with electron tracks incompatible with conversion tracks are rejected.

In the kinematic range considered by the analysis, the efficiency of the identification criteria, is above 90(85)% for prompt isolated photon candidates in the barrel (endcaps). The identification and trigger efficiencies are measured using events containing a pair of electrons or a di-muon pair in association with a photon. The efficiencies measured in data are found to be compatible with the predicted ones within uncertainties.

The fraction of events where more than one diphoton pair satisfies the selection criteria is roughly 1%. In these cases, only the pair with the largest scalar sum of photon momenta is retained. Diphoton pairs are split into two category: the first, denoted "EBEB" in the following, contains pairs where both candidates are reconstructed in the ECAL barrel, while the second, denoted "EBEE", contains pairs where one of the candidates is reconstructed in the ECAL endcaps. The fraction of graviton events selected in each of the analysis categories is shown in

Fig. 1 for different mass and $\tilde{\kappa}$ hypotheses.

The selection criteria were optimised using simulated signal and background samples and fixed prior to inspecting the diphoton invariant mass distribution in the search region, which is defined as $m_{\gamma\gamma} > 500\,\text{GeV}$. The level of agreement between data and simulation was assessed before inspecting the diphoton invariant mass distribution in the signal region. To do so, other distributions in the search region, as well as all distributions for events outside of the search region were inspected. The event selection efficiencies and the background composition were measured in data and compared with expectations. Finally, the ratio between the total number of expected and observed events and the ratio between the expected and observed fraction of irreducible background in the search region were checked as part of the procedure. None of these assessments lead to a change in the selection criteria that were determined using simulated events.

5 Determination of the photon energy scale and resolution

As described above, the energy of the photon candidates is assigned using a multi-variate regression. The corrections are tuned on photon candidates mostly of lower energies than those entering the analysis. For this reason, the energy scale of photons above $\sim 200\,\text{GeV}$ slightly deviates from unity. The residual shift, due to the energy dependence of the longitudinal non-containment of the photon shower, is below 0.5% up to energies of $\sim 500\,\text{GeV}$ and below 1% up to energies of $\sim 1.5\,\text{TeV}$.

Discrepancies in the photon energy scale and resolution between data and simulation are resolved using dielectron events. Energy scale and resolution corrections are derived primarily from $Z \to e^+e^-$ events, using the procedure described in Ref.[21]. The corrections are derived in eight bins defined in terms of the R_9 variable (defined as the ratio between the energy deposited in the central 3x3 crystal matrix and the full cluster energy) and of $|\eta_{SC}|$.

The size of the energy scale corrections derived from $Z \to e^+e^-$ events is of the order of $0.5(1.5)\%$ for photon candidates in the barrel (endcaps) region, while the additional Gaussian smearing needed to match the energy resolution in simulated events with that in data is of the order of $1.5(3)\%$ in the barrel (endcaps). The dielectron invariant mass distribution obtained, for data and simulated events, after the adjustment procedure is shown in Fig. 2. For signal hypotheses corresponding to $\tilde{\kappa} = 0.01$ and $m_G < 1\,\text{TeV}$, the expected exclusion limit on the graviton production cross section using the resolution corrections is 10-15% less stringent than that anticipated after deriving single-channel response calibration coefficients from 13 TeV data.

The evolution of the correction factors as a function of energy of the photon candidate is assessed using dielectron events produced in the Drell-Yan process. Pairs of electron candidates with an invariant mass above 200 GeV are considered. The transverse momentum of the dielectron system is required to be below 10 GeV and the selected events are used to derive residual energy scale and resolution corrections.

A fit procedure analogous to the one described in Ref.[21] is applied. The distributions of two different variables are used. For the energy corrections, the distribution of the quadratic sum of the electron transverse momenta is used. For the resolution corrections, the ratio of the two momenta is used.

Separate residual energy scale and resolution corrections are derived for clusters in the barrel and endcap regions. All residual corrections are found to be compatible with zero within the associated statistical uncertainties, which are about 0.5%.

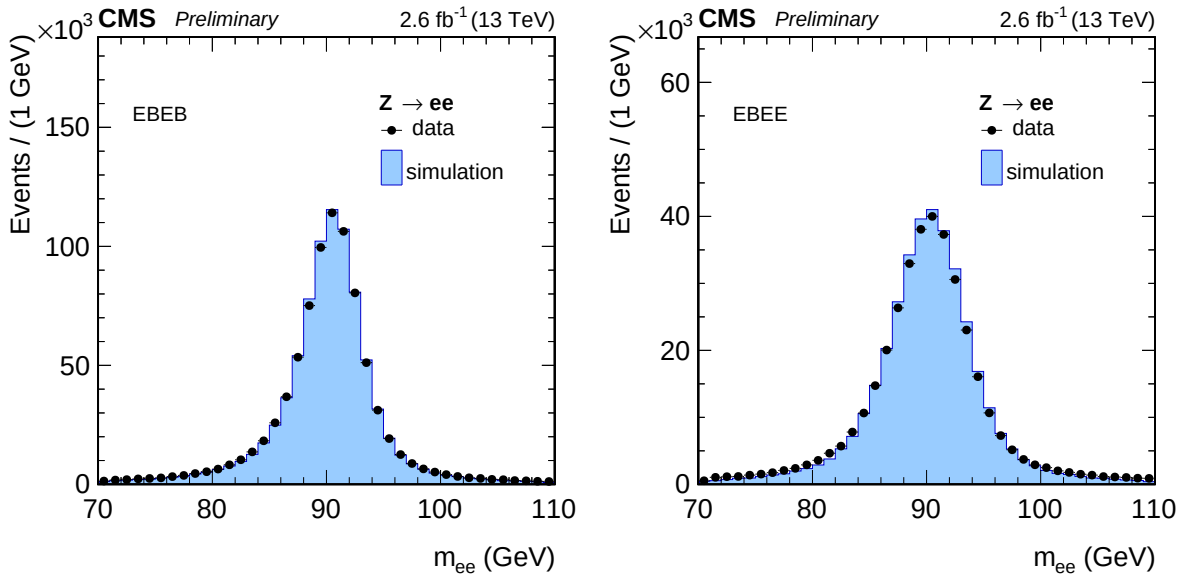

Figure 2: Comparison between the predicted and observed invariant mass distribution of electron pairs obtained after the application of energy scale and resolution corrections. Distributions are shown for events where both electrons are reconstructed in the barrel (left) and events where one electron is in the endcaps (right). The simulation predictions are scaled to match the number of events observed in data.

6 Diphoton mass spectrum

In the data sample, a total of 1218 (596) diphoton pairs are selected in the EBEB (EBEE) category. Out of these, 97 (163) pairs have an invariant mass above 500 GeV.

The invariant mass distribution of the selected events is shown in Fig. 3. A parametrisation of the spectrum of the form $f(m_{\gamma\gamma}) = m_{\gamma\gamma}^{a+b\cdot\log(m_{\gamma\gamma})}$, obtained through a maximum likelihood fit to the selected events, is shown. This parametric form corresponds to the one chosen to model the background in the hypothesis tests, as detailed in Section 9.

The composition of the background entering the final selection is determined through a bi-dimensional template fit in the plane $I_{Ch}(\gamma^1)$, $I_{Ch}(\gamma^2)$. For this purpose, the selection criterion on I_{Ch} is relaxed to include all the events in which both photon candidates have I_{Ch} below 15 GeV. A three component fit is then performed to separate the contribution of events with two prompt photons ($\gamma\gamma$) from those where one (γj) or two (jj) of the photon candidates arises from the fragmentation of an hadronic jet. The invariant mass spectrum of the EBEB (EBEE) category is subdivided in 10 (7) bins and the template fit repeated in each bin. This fit was performed prior to the inspection of the diphoton invariant mass distribution in the search region and the search region was analysed as a single bin.

The techniques used in the analysis to derive the shape of the different background components closely follow those used in Ref. [31]. The isolation spectrum of prompt isolated photons is extracted randomly sampling the contribution of the pile-up and underlying event to I_{Ch}. For photon candidates resulting from jet fragmentation, the isolation distribution is obtained by inverting the requirement on the transverse size of the electromagnetic cluster. In the case of the $\gamma\gamma$ component, the template distributions are built by randomly sampling the events entering in the fit, up to nine times for each photon candidate. Photon candidates from different events are combined to construct the γj and jj templates shape. In this procedure, the properties of the

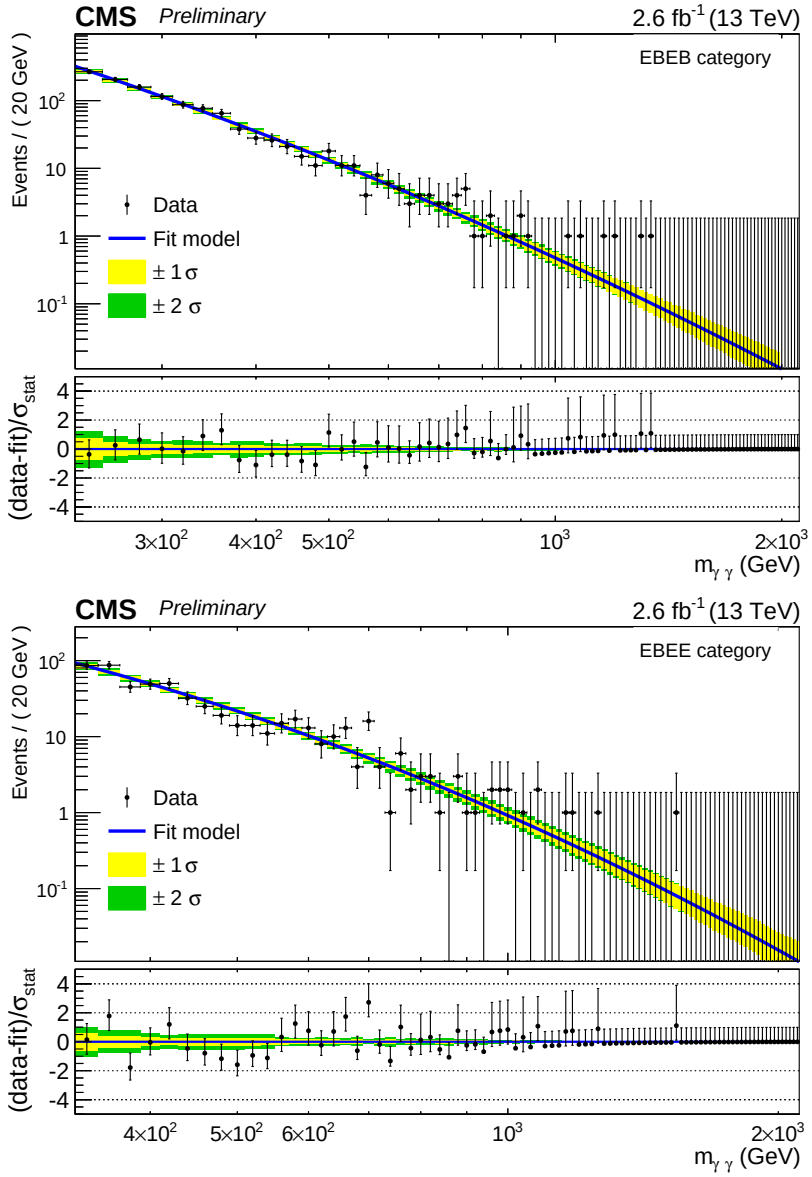

Figure 3: Observed invariant mass spectrum for the EBEB (top) and EBEE (bottom). The results of parametric fits to the data are also shown.

photon candidates are matched to those selected in the analysis using a k-nearest-neighbours algorithm, with k=10.

Figure 4 shows, in $m_{\gamma\gamma}$ bins, the measured contributions of the different background components in the region $I_{Ch} < 5\,\text{GeV}$. It can be seen that the dominant component, accounting for more than 90(80)% of the selected events in the EBEB (EBEE) category, is represented by the irreducible $\gamma\gamma$ background.

The spectrum of the irreducible background extracted through the procedure described above is then compared with the predictions extracted by rescaling the mass spectrum predicted by the Sherpa generator to the one extracted from the 2γNNLO program [32]. The result of the comparison is shown in Fig. 5. The mass spectra predicted by the simulation are in good agreement with the one seen in data.

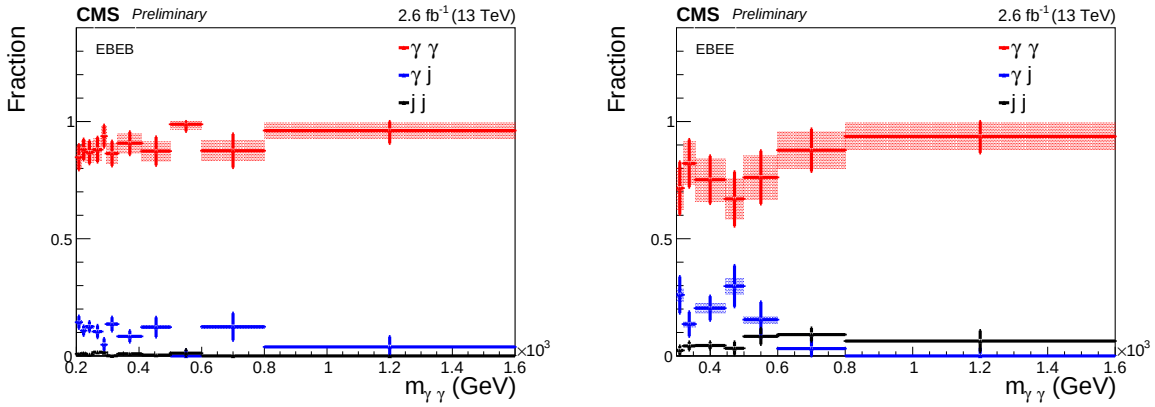

Figure 4: Measured composition of the background for the EBEB (left) and EBEE (right) categories.

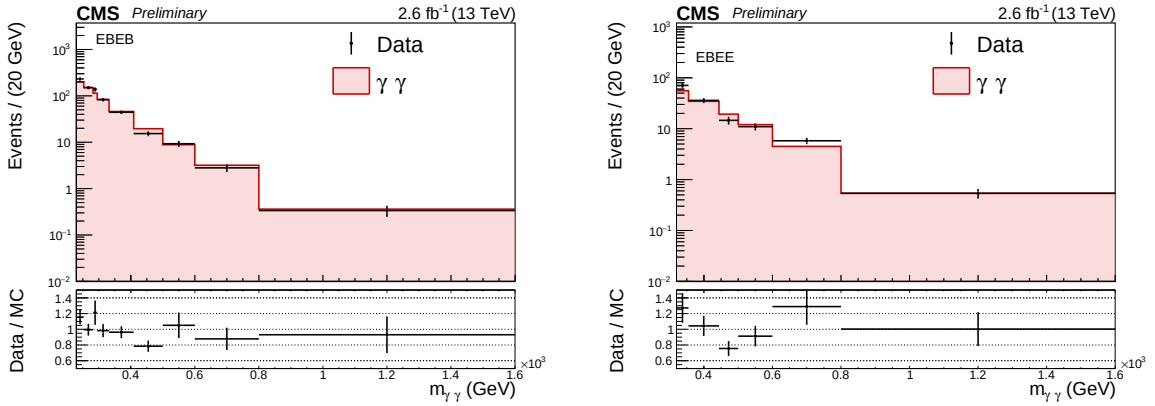

Figure 5: Comparison between the measured and the predicted invariant mass spectrum of the non resonant $\gamma\gamma$ background for the EBEB (left) and EBEE (right) categories.

7 Statistical analysis

The results of the search are interpreted in the frame of a composite statistical hypothesis test. A simultaneous fit to the invariant mass spectra of the the EBEB and EBEE event categories is used to study the compatibility of the data with the background-only and the signal+background hypotheses.

The test statistics used in the hypothesis tests are based on the profile likelihood ratio:

$$q(\mu) = -2log\frac{L(\mu \cdot S + B|\hat{\underline{\theta}}_\mu)}{L(\hat{\mu} \cdot S + B|\hat{\underline{\theta}})}$$

Where S and B are the probability density functions for the graviton and the SM backgrounds respectively, μ is the so-called "signal strength" parameter and $\underline{\theta}$ are the nuisance parameters of the model, used to model systematic uncertainties. The $\hat{x}$ notation indicates the best-fit value of the parameter x, while the notation $\hat{x}_y$ denotes the best-fit value of x conditional on y.

m_G (GeV)	category	$\tilde{\kappa}$	FWHM (GeV)	$\tilde{\kappa}$	FWHM (GeV)
500	EBEB	0.01	14	0.2	36
500	EBEE	0.01	22	0.2	42
1000	EBEB	0.01	27	0.2	74
1000	EBEE	0.01	43	0.2	85
2000	EBEB	0.01	54	0.2	147
2000	EBEE	0.01	76	0.2	163
3000	EBEB	0.01	96	0.2	225
3000	EBEE	0.01	110	0.2	254
4000	EBEB	0.01	121	0.2	320
4000	EBEE	0.01	150	0.2	326

Table 1: Width of the reconstructed mass distribution for different signal hypotheses.

8 Signal modelling

The signal distribution in $m_{\gamma\gamma}$ is determined from the convolution of the intrinsic shape of the resonance and the ECAL detector response. The intrinsic shape of the graviton signal is derived using the PYTHIA generator. A fine grid of mass points with 125 GeV spacing is used and the resulting shapes interpolated to intermediate points using the "moment morphing" technique described in [33]. The detector response is determined using fully simulated graviton samples of small intrinsic width and corrected for the additional Gaussian smearing determined from dielectron events. Nine equidistant mass hypotheses in the range 500-4500 GeV are employed.

In order to determine the signal normalisation, the efficiency of the final event selection is combined with the kinematic acceptance. The first is obtained from fully simulated samples and interpolated using a quadratic function of the resonance mass. The second is obtained from the finely spaced grid of samples and parametrised as a quadratic function of both the resonance mass and $\tilde{\kappa}$. A summary of the width of the signal reconstructed mass distribution, quantified through its full width at half maximum is reported in Table 1, while the function accounting for selection efficiency and acceptance is shown in Fig. 1.

9 Background modelling

The background $m_{\gamma\gamma}$ spectrum is described by a parametric function of $m_{\gamma\gamma}$. The parametric coefficients are obtained from a fit to the data events, and considered as unconstrained nuisance parameters in the hypothesis test, allowing the building a data-driven description of the shape.

The accuracy of the background determination is assessed using MC simulations and it is quantified by studying the difference between the true and predicted number of background events in 14 $m_{\gamma\gamma}$ windows in the search region. Pseudo-experiments are drawn from the mass spectrum predicted by MC simulation. The total number of events in each pseudo-experiment is taken from a Poisson distribution where the mean is determined by the observation in data.
For each mass window, the distribution of the pull variable, defined as the difference between the true and predicted number of events divided by the estimated statistical uncertainty, is constructed. If the absolute value of the median of this distribution is not found to be below 0.5 in a window, an additional uncertainty is assigned to the background parametrisation. A modified pull distribution is then constructed increasing the statistical uncertainty on the fit by an extra term, denoted as bias term, which is parametrised as a smooth function of $m_{\gamma\gamma}$, tuned in such a way that the absolute value of the median of the modified pull distribution is below 0.5 for all regions.

In order to account for this uncertainty in the hypothesis test, a signal-like term is added to the background model. The normalisation of such a term is taken to be normally distributed with a width determined by the integral of the bias term over the full-width at half-maximum of the tested signal shape.

10 Systematic uncertainties

In this analysis the impact of the systematic uncertainties is smaller than that of the statistical uncertainties. The parametric background model has no associated systematic uncertainties, except for the bias term uncertainty described above. The shape coefficients are treated as unconstrained nuisance parameters and contribute to the statistical uncertainty.

Uncertainties associated to the signal modelling are summarised here:

- Luminosity uncertainty: a 4.6% on the signal normalisation is assigned to reflect the uncertainty on the knowledge of the total integrated luminosity.
- Trigger and photon identification uncertainties: a 10% uncertainty on the signal normalisation is included to account for the uncertainty in the knowledge of the data/MC scale factors.
- Parton distribution functions: a 6% uncertainty on the signal normalisation is assigned to account for the variation in the kinematic acceptance of the analysis coming from the use of alternative PDF sets.
- Photon energy scale uncertainty: a 1% systematic uncertainty is assigned to the knowledge of the photon energy scale in the range considered by the analysis.

11 Results

To set upper limits on the graviton production rate, the modified frequentist method, commonly known as CL_s is used following the prescription in Ref. [34]. Asymptotic formulae [35] are used in the calculation. The validity of such formulae in the regime of this analysis was verified for a subset of the hypothesis tests. Expected and observed upper limits on $\sigma_G \cdot BR_{\gamma\gamma}$ are shown in Fig. 6 for values $\tilde{\kappa}$ of 0.01, 0.1 and 0.2. Using leading order cross sections obtained with PYTHIA, RS gravitons of mass below 1.35, 3.1 and 3.8 TeV are expected to be excluded by the analysis for $\tilde{\kappa}$ of 0.01 0.1 and 0.2 respectively. As a result of the observation, for $\tilde{\kappa} = 0.01$, values of m_G below 1.3 TeV are excluded. For $\tilde{\kappa}$ = 0.1 and 0.2, gravitons masses below 3.1 and 3.8 TeV are excluded by the analysis.

The compatibility of the observation with the background-only hypothesis is evaluated computing the background only p-value. The latter is defined as the probability, in the background-only hypothesis, for $q(0)$ to be above the observation. This quantity, the "local p-value" p_0, does not take into account the fact that many signal hypotheses are tested. Asymptotic formulas are used to compute p_0 as a function of the graviton mass and width hypotheses. The validity of the formulas has been verified for a subset of the points.

The value of p_0 for different signal hypotheses is shown in Fig. 7. The largest excess observed in data has a p_0 value corresponding to 2.6 standard deviations, it is observed for $m_G = 760$ GeV and $\tilde{\kappa} = 0.01$ and is determined by an excess of events in the EBEB category. The probability of observing an excess more significant than this for at least one of the mass hypotheses with $\tilde{\kappa} = 0.01$ is estimated using the procedure described in Ref. [36]. The significance of the excess is estimated to be less than 1.2 standard deviations after taking this into account. Such a signif-

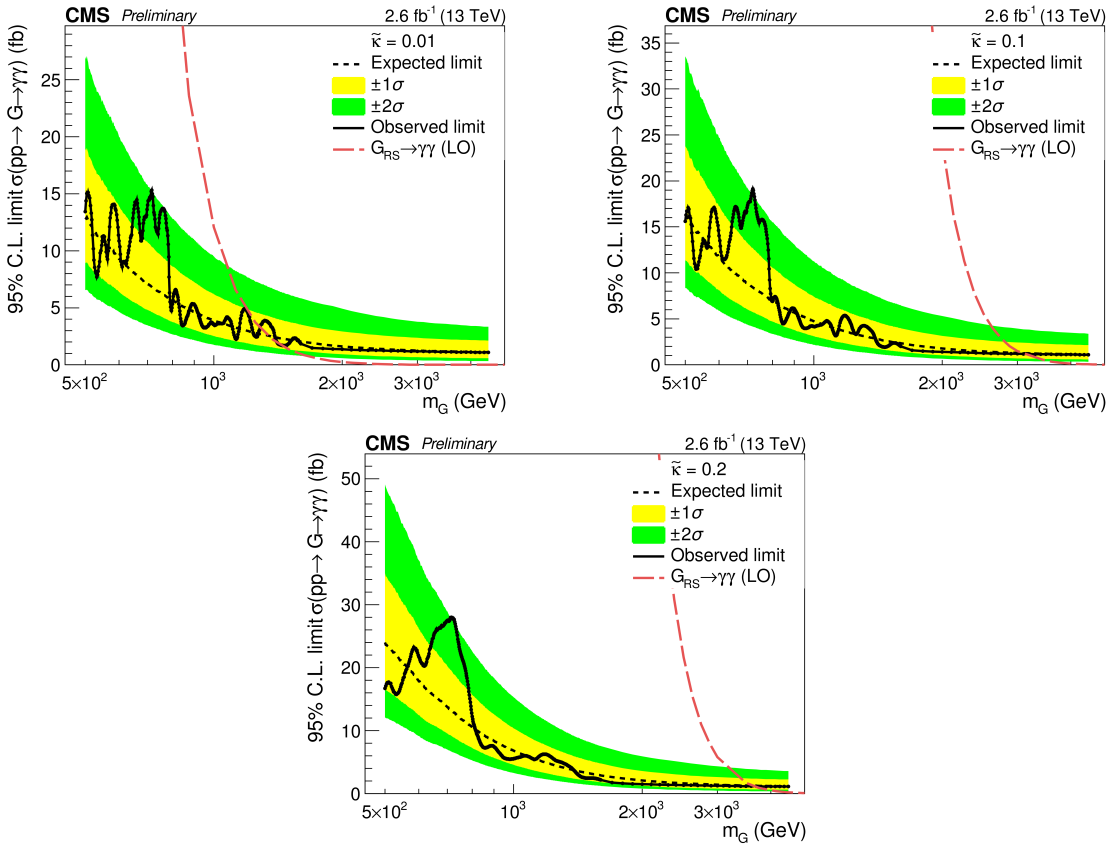

Figure 6: Expected and observed 95% C.L. exclusion limits for different signal hypotheses. The range 500 GeV $< m_{\mathrm{G}} <$ 4.5 TeV is shown for $\tilde{\kappa} = 0.01, 0.1, 0.2$ on the top-left, top-right, bottom respectively.

icance is expected to reduce further after accounting for the fact that several $\tilde{\kappa}$ hypotheses have been searched for.

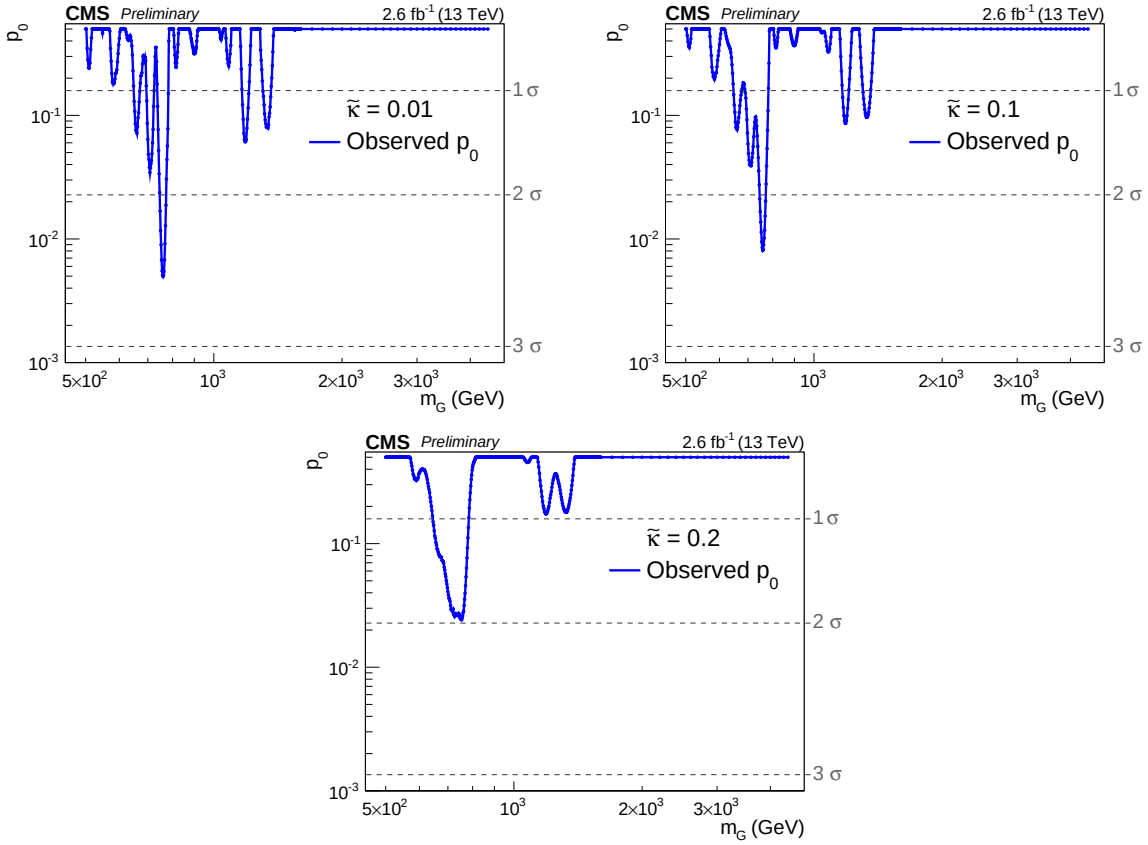

Figure 7: Observed background-only p-value for different signal hypotheses. The range $500\,\text{GeV} < m_\text{G} < 4.5\,\text{TeV}$ is shown for $\tilde{\kappa} = 0.01, 0.1, 0.2$ on the top-left, top-right, bottom respectively.

12 Summary

A search for new physics using the diphoton mass spectrum has been presented. The analysis is based on 2.6 fb^{-1} of pp collisions collected by the CMS experiment in 2015 at $\sqrt{s} = 13$ TeV. Events containing two photon candidates with transverse momenta above 75 GeV were selected. The mass spectrum above 500 GeV was inspected to search for the production of spin-2 resonances, predicted in the context of extradimensional models. Data driven techniques were applied to characterise and model the the SM diphoton production, as well as the background arising from jets. The observed mass distribution was found to be consistent with the expectations from the SM. Limits on the production of Randall-Sundrum gravitons of mass $500\,\text{GeV} < m_G < 4.5\,\text{TeV}$ and $\tilde{\kappa} < 0.2$ were set using the modified frequentist approach.

The largest excess in data sample is observed for $m_G = 760\,\text{GeV}$ and $\tilde{\kappa} = 0.01$, has a local significance 2.6 standard deviations and a global significance smaller than 1.2 standard deviations. Using leading order cross sections obtained with PYTHIA, RS gravitons of mass below 1.35, 3.1 and 3.8 TeV are expected to be excluded by the analysis for $\tilde{\kappa}$ of 0.01, 0.1 and 0.2 respectively. As a result of the observation, for $\tilde{\kappa} = 0.01$, values of m_G below 1.3 TeV are excluded. For $\tilde{\kappa}$ = 0.1 and 0.2, gravitons masses below 3.1 and 3.8 TeV are excluded by the analysis. These limits exceed those obtained by previous analyses.

References

[1] ATLAS Collaboration, "Observation of a new particle in the search for the Standard Model Higgs boson with the ATLAS detector at the LHC", *Phys. Lett.* **B716** (2012) 1–29, doi:10.1016/j.physletb.2012.08.020, arXiv:1207.7214.

[2] CMS Collaboration, "Observation of a new boson at a mass of 125 GeV with the CMS experiment at the LHC", *Phys. Lett.* **B716** (2012) 30–61, doi:10.1016/j.physletb.2012.08.021, arXiv:1207.7235.

[3] N. Arkani-Hamed, S. Dimopoulos, and G. Dvali, "The Hierarchy problem and new dimensions at a millimeter", *Phys.Lett.* **B429** (1998) 263–272, doi:10.1016/S0370-2693(98)00466-3, arXiv:hep-ph/9803315.

[4] L. Randall and R. Sundrum, "A Large mass hierarchy from a small extra dimension", *Phys. Rev. Lett.* **83** (1999) 3370–3373, doi:10.1103/PhysRevLett.83.3370, arXiv:hep-ph/9905221.

[5] G. F. Giudice, R. Rattazzi, and J. D. Wells, "Quantum gravity and extra dimensions at high-energy colliders", *Nucl. Phys.* **B544** (1999) 3–38, doi:10.1016/S0550-3213(99)00044-9, arXiv:hep-ph/9811291.

[6] E. A. Mirabelli, M. Perelstein, and M. E. Peskin, "Collider signatures of new large space dimensions", *Phys. Rev. Lett.* **82** (1999) 2236–2239, doi:10.1103/PhysRevLett.82.2236, arXiv:hep-ph/9811337.

[7] T. Han, J. D. Lykken, and R.-J. Zhang, "On Kaluza-Klein states from large extra dimensions", *Phys. Rev.* **D59** (1999) 105006, doi:10.1103/PhysRevD.59.105006, arXiv:hep-ph/9811350.

[8] J. L. Hewett, "Indirect collider signals for extra dimensions", *Phys. Rev. Lett.* **82** (1999) 4765–4768, doi:10.1103/PhysRevLett.82.4765, arXiv:hep-ph/9811356.

[9] H. Davoudiasl, J. L. Hewett, and T. G. Rizzo, "Phenomenology of the Randall-Sundrum Gauge Hierarchy Model", *Phys. Rev. Lett.* **84** (2000) 2080, doi:10.1103/PhysRevLett.84.2080, arXiv:hep-ph/9909255.

[10] CMS Collaboration Collaboration, "Search for High-Mass Diphoton Resonances in pp Collisions at $\sqrt{s} = 8$ TeV with the CMS Detector", CMS Physics Analysis Summary CMS-PAS-EXO-12-045, CERN, 2015.

[11] ATLAS Collaboration, "Search for high-mass diphoton resonances in pp collisions at $\sqrt{s} = 8$ TeV with the ATLAS detector", *Phys. Rev.* **D92** (2015), no. 3, 032004, doi:10.1103/PhysRevD.92.032004, arXiv:1504.05511.

[12] ATLAS Collaboration, "Search for Extra Dimensions in diphoton events using proton-proton collisions recorded at $\sqrt{s} = 7$ TeV with the ATLAS detector at the LHC", *New J. Phys.* **15** (2013) 043007, doi:10.1088/1367-2630/15/4/043007, arXiv:1210.8389.

[13] CMS Collaboration, "Search for signatures of extra dimensions in the diphoton mass spectrum at the Large Hadron Collider", *Phys. Rev. Lett.* **108** (2012) 111801, doi:10.1103/PhysRevLett.108.111801, arXiv:1112.0688.

[14] ATLAS Collaboration, "Search for high-mass dilepton resonances in pp collisions at $\sqrt{s} = 8$ TeV with the ATLAS detector", *Phys. Rev.* **D90** (2014), no. 5, 052005, doi:10.1103/PhysRevD.90.052005, arXiv:1405.4123.

[15] CMS Collaboration, "Search for heavy narrow dilepton resonances in pp collisions at $\sqrt{s} = 7$ TeV and $\sqrt{s} = 8$ TeV", *Phys. Lett.* **B720** (2013) 63–82, doi:10.1016/j.physletb.2013.02.003, arXiv:1212.6175.

[16] CMS Collaboration, "Search for narrow resonances using the dijet mass spectrum in pp collisions at $\sqrt{s}$=8 TeV", *Phys. Rev.* **D87** (2013), no. 11, 114015, doi:10.1103/PhysRevD.87.114015, arXiv:1302.4794.

[17] ATLAS Collaboration, "Search for new phenomena in the WW to $\ell\nu\ell'\nu'$ final state in pp collisions at $\sqrt{s} = 7$ TeV with the ATLAS detector", *Phys. Lett.* **B718** (2013) 860–878, doi:10.1016/j.physletb.2012.11.040, arXiv:1208.2880.

[18] CDF Collaboration, "Search for New Dielectron Resonances and Randall-Sundrum Gravitons at the Collider Detector at Fermilab", *Phys. Rev. Lett.* **107** (2011) 051801, doi:10.1103/PhysRevLett.107.051801, arXiv:1103.4650.

[19] D0 Collaboration, "Search for Randall-Sundrum gravitons in the dielectron and diphoton final states with 5.4 fb^{-1} of data from $p\bar{p}$ collisions at $\sqrt{s} = 1.96$ TeV", *Phys. Rev. Lett.* **104** (2010) 241802, doi:10.1103/PhysRevLett.104.241802, arXiv:1004.1826.

[20] CMS Collaboration, "The CMS experiment at the CERN LHC", *JINST* **3** (2008) S08004, doi:10.1088/1748-0221/3/08/S08004.

[21] CMS Collaboration, "Performance of photon reconstruction and identification with the CMS detector in proton-proton collisions at $\sqrt{s} = 8$ TeV", *JINST* **10** (2015) P08010, doi:10.1088/1748-0221/10/08/P08010, arXiv:1502.02702.

[22] CMS Collaboration, "Particle-flow event reconstruction in CMS and performance for jets, taus, and $E_{\mathrm{T}}^{\mathrm{miss}}$", CMS Physics Analysis Summary CMS-PAS-PFT-09-001, 2009.

[23] CMS Collaboration, "Commissioning of the particle-flow event with the first LHC collisions recorded in the CMS detector", CMS Physics Analysis Summary CMS-PAS-PFT-10-001, 2010.

[24] T. Sjstrand et al., "An Introduction to PYTHIA 8.2", *Comput. Phys. Commun.* **191** (2015) 159–177, doi:10.1016/j.cpc.2015.01.024, arXiv:1410.3012.

[25] R. D. Ball et al., "Parton distributions with LHC data", *Nucl. Phys.* **B867** (2013) 244–289, doi:10.1016/j.nuclphysb.2012.10.003, arXiv:1207.1303.

[26] T. Gleisberg et al., "Event generation with SHERPA 1.1", *JHEP* **02** (2009) 007, doi:10.1088/1126-6708/2009/02/007, arXiv:0811.4622.

[27] J. Alwall et al., "The automated computation of tree-level and next-to-leading order differential cross sections, and their matching to parton shower simulations", *JHEP* **07** (2014) 079, doi:10.1007/JHEP07(2014)079, arXiv:1405.0301.

[28] NNPDF Collaboration, "Parton distributions for the LHC Run II", *JHEP* **04** (2015) 040, doi:10.1007/JHEP04(2015)040, arXiv:1410.8849.

[29] CMS Collaboration, "Event generator tunes obtained from underlying event and multiparton scattering measurements", arXiv:1512.00815.

[30] GEANT4 Collaboration, "GEANT4 - a simulation toolkit", *Nucl. Instrum. Meth. A* **506** (2003) 250, doi:10.1016/S0168-9002(03)01368-8.

[31] CMS Collaboration, "Measurement of differential cross sections for the production of a pair of isolated photons in pp collisions at $\sqrt{s} = 7$ TeV", *Eur.Phys.J.* **C74** (2014), no. 11, 3129, doi:10.1140/epjc/s10052-014-3129-3, arXiv:1405.7225.

[32] S. Catani et al., "Diphoton production at hadron colliders: a fully-differential QCD calculation at NNLO", *Phys.Rev.Lett.* **108** (2012) 072001, doi:10.1103/PhysRevLett.108.072001, arXiv:1110.2375.

[33] M. Baak, S. Gadatsch, R. Harrington, and W. Verkerke, "Interpolation between multi-dimensional histograms using a new non-linear moment morphing method", *Nucl. Instrum. Meth. A* **771** (2015) 39, doi:10.1016/j.nima.2014.10.033, arXiv:1410.7388.

[34] ATLAS and CMS Collaborations, LHC Higgs Combination Group, "Procedure for the LHC Higgs boson search combination in Summer 2011", ATL-PHYS-PUB/CMS NOTE 2011-11, 2011/005, 2011.

[35] G. Cowan, K. Cranmer, E. Gross, and O. Vitells, "Asymptotic formulae for likelihood-based tests of new physics", *Eur.Phys.J.* **C71** (2011) 1554, doi:10.1140/epjc/s10052-011-1554-0, 10.1140/epjc/s10052-013-2501-z, arXiv:1007.1727.

[36] E. Gross and O. Vitells, "Trial factors or the look elsewhere effect in high energy physics", *Eur. Phys. J.* **C70** (2010) 525–530, doi:10.1140/epjc/s10052-010-1470-8, arXiv:1005.1891.